J. Math. Computer Sci., 27 (2022), 1–17

Online: ISSN 2008-949X

Journal of Mathematics and Computer Science

Journal Homepage: www.isr-publications.com/jmcs

Outbreak spatial pattern formation based on an SI model with the infected cross-diffusion term

A. Triska*, A. Y. Gunawan, N. Nuraini

Department of Mathematics, Faculty of Mathematics and Natural Sciences, Institut Teknologi Bandung, Jl. Ganesha No. 10, Bandung, West Java, 40116, Indonesia.

Abstract

This study is to discuss the pattern formations of a spatial epidemic model with cross-diffusion of the susceptible and infected groups simultaneously. The infected cross-diffusion term described the situation that the infected was allowed to move to areas with high density of the susceptible such as for work or study, especially after the pandemic. Turing analysis was applied to the model and yielded the conditions for Turing instability corresponding to the model. The amplitude equations were also given by the support of multiple-scale analysis, which then provided information about the stability of the patterns near the Turing bifurcation point. Numerical simulations revealed that there were five types of patterns, such as the spots, spots-stripes, stripes, stripes-holes, and holes. The holes indicated a disease outbreak in a region, while the spots showed non-outbreak. Furthermore, numerical simulations were carried out by varying the cross-diffusion coefficients of the susceptible and infected. The simulation results showed once the cross-diffusion coefficient of the infected was bigger than the susceptible, then an outbreak in a region was triggered. The results of this study showed that the movement of infected had a significant role in the spread of an infectious disease that could lead to another wave of pandemic. By using Turing analysis as a tool, as well as predator-prey model as the basis of movement theory, this paper tries to fill in the gaps in the discussion about the movement of infected people to areas with high density of the susceptible.

Keywords: Cross-diffusion of the infected, spatial epidemic model, Turing pattern, Turing bifurcation, amplitude equations.

2020 MSC: 35B36, 92B05, 37D99, 92D25, 35K57, 92D30.

1. Introduction

In 1952, Turing [38] discovered that in a reaction-diffusion system, a homogeneous steady state which is stable to small temporal perturbation under the absence of diffusion becomes unstable in the presence of diffusion term [30]. This phenomenon is known as Turing instability. This instability generates a pattern on the spatial domain called Turing patterns. After this discovery, many researchers were inspired to apply his concept to study the pattern formation in various fields such as physical, chemical, biological, and ecological processes [9, 13, 21, 23, 32].

The study of the spread of infectious diseases through mathematical models has been around for a long time. Recently, an epidemic model was developed by introducing spatial dependence through a

*Corresponding author
Email address: a.triska@s.itb.ac.id, anit.triska@gmail.com (A. Triska)

doi: 10.22436/jmcs.027.01.01

Received: 2021-08-14 *Revised:* 2021-10-25 *Accepted:* 2021-12-01

reaction-diffusion system known as the spatial epidemic model. Many researchers have studied spatial epidemic models with self-diffusion alone [2, 6, 35, 39, 40, 42, 44]. Cross-diffusion of the susceptible is also applied to the spatial epidemic model. This term represents the tendency of the susceptible to stay away from the infected since they are able to recognize the infected [4, 5, 12, 24, 37, 41, 43]. The results of this study indicate that susceptible cross-diffusion has an influence on the spread of an infectious disease and the pattern dynamics.

The diffusion term is also widely applied by researchers to predator-prey models with self-diffusion only [8, 20, 27, 46, 49, 50] and with cross-diffusion as well [1, 3, 14–19, 28, 34, 45]. In order to describe their behavior in nature, the predator-prey models in [3, 14, 28, 45] considered both of cross-diffusion of the predator and prey simultaneously. They apply positive values to all diffusion coefficients. They considered the positive value of the prey cross-diffusion coefficient to indicate that the prey was approaching a lower predator concentration. However, in most cases, predators choose to avoid the group defense with large numbers of prey and prefer to capture them from smaller concentration groups. Therefore, the predator cross-diffusion coefficient was also chosen as a positive value which means that predators tend to spread towards lower prey concentrations [14].

When spatially heterogeneous interventions are considered, it is clearly important to represent the site of infection and the pattern of transmission [31]. The infection will increase as the movement expands. From biological point of view, people can also move to areas of high density of the susceptible because of various reasons such as for work or study. However, it is risky to allow infected people moving freely to areas with high density of the susceptible, especially after the pandemic. For an example, in the current situation where people infected with the Coronavirus disease (Covid-19) who experience mild symptoms can carry out daily activities in areas with high density of the susceptible or even travel to urban areas. When people start to feel it is safe to travel, meet people, do routine work, even though they are still infected, that's the time when the pandemic can outbreak again like in India and Japan [22, 23].

Determining the end of the pandemic is crucial. A premature decision to declare that the pandemic has reached its end can cause from dangerous to deadly euphoria in society. To prevent this to happen again, there must be a study on the behavior patterns of people moving who are still infected, from one place to another especially to areas with high density of the susceptible such as for work or study. As a result, this study addresses a spatial epidemic model, not only with cross-diffusion of the susceptible as in previous studies [4, 5, 12, 24, 37, 43], but also with cross-diffusion of the infected to illustrate the above-mentioned situation. The diffusion coefficient can be positive, zero or negative [16, 37, 40]. A positive value is applied to the cross-diffusion coefficient of susceptible denotes movement of the susceptibles in a direction of lower density of infecteds which implies that susceptible tends to stay away from the infected [4, 5, 12, 24, 37, 43]. Meanwhile, in contrast to the perspective of the predator-prey model in [14, 28, 45], we apply a negative value to the cross-diffusion coefficient of the infected as it implies that the infected move towards a higher density of susceptibles.

Another important work in this study is the amplitude equations, which are tools in understanding pattern formation scenarios in reaction-diffusion systems near the threshold of the Turing bifurcation parameter [7, 11]. The homogeneous steady state of the system becomes unstable because of small heterogeneous perturbations via Turing instability. The transition from a stationary-homogeneous-steady-state to a spatially-heterogeneous-pattern near the Turing bifurcation boundary takes a significant long amount of time [46]. Therefore, multiple scale perturbation analysis was used to derive the amplitude equations to study the dynamics of this active slow mode [49]. These theoretical results are compared with numerical simulations. Furthermore, patterns were observed for various values of the cross-diffusion coefficient, to ascertain the effect of competition on susceptible and infected movements.

According to the introduction above, this study will focus on the Turing pattern of the spatial epidemic model because of the variation of the cross-diffusion coefficient, especially the infected. This paper is organized as follows. In the next section, we will present a spatial epidemic model with cross-diffusion of susceptible and infected, followed by a Turing analysis in Section 3. In Section 4, the amplitude equations are derived. Numerical simulations are carried out to verify the analysis, which is presented in Section 5.

Finally, we briefly provide conclusions and remarks. The results of this study can be the basis of reliable decision.

2. Mathematical model

Assume that an epidemic SI model, with logistic growth in the susceptible with cross-diffusion of the susceptible and infected, is written as follows

$$\begin{aligned}\frac{\partial S}{\partial t} &= rS\left(1-\frac{S}{K}\right)-\beta\frac{SI}{S+I}+D_S\nabla^2 S+D_1\nabla^2 I,\\ \frac{\partial I}{\partial t} &= \beta\frac{SI}{S+I}-\eta I+D_I\nabla^2 I-D_2\nabla^2 S,\end{aligned} \tag{2.1}$$

with the positive initial conditions

$$S(x,y,0)>0,\quad I(x,y,0)>0,\quad (x,y)\in\Omega.$$

The D_S and D_I are self-diffusion coefficients, while D_1 and D_2 are cross-diffusion coefficients of the susceptible and infected, respectively. All diffusion coefficients are taken to be positive. Note that, the sign in front of D_2 is taken to be negative since this term implies that the infected tends to move towards higher densities of the susceptible.

The Ω is a spatial domain in R^2 and $\nabla^2=\frac{\partial^2}{\partial x^2}+\frac{\partial^2}{\partial y^2}$ is the Laplacian operator in two-dimensional spaces [25, 36]. Here, $S(x,y,t)$ and $I(x,y,t)$ are the population densities of the susceptible and infected at (x,y) at time t in Ω with the size $L\times L$, respectively. The parameters r,β,η, and K are positive constants that represent the intrinsic growth rate of S, the infection rate, the death rate of I, and carrying capacity, respectively. Model (2.1) is evaluated under zero flux boundary condition

$$\frac{\partial S}{\partial \mathbf{n}}=0,\quad \frac{\partial I}{\partial \mathbf{n}}=0,\quad (x,y)\in\partial\Omega, \tag{2.2}$$

where $\mathbf{n}$ is the outward unit normal vector of the smooth boundary $\partial\Omega$. The notations $\frac{\partial S}{\partial \mathbf{n}}$ and $\frac{\partial I}{\partial \mathbf{n}}$ represent the change of the number of S and I against normal vectors, respectively. This study focuses on considering self-organization in generating the pattern, so that zero flux boundary condition is chosen since the system is assumed to be closed, i.e., no incoming or outgoing population movement across the boundary. Redefining

$$S^*=\frac{S}{K},\quad I^*=\frac{I}{K},\quad x^*=\frac{x}{L},\quad y^*=\frac{y}{L},\quad t^*=\frac{D_I t}{L^2},$$

model (2.1) can be transformed into a dimensionless form. For convenience, removing the asterisks notation in the dimensionless form of model (2.1), the following is obtained

$$\begin{aligned}\frac{\partial S}{\partial t} &= \gamma f(S,I)+d\nabla^2 S+\xi_1 d\nabla^2 I,\\ \frac{\partial I}{\partial t} &= \gamma g(S,I)+\nabla^2 I-\xi_2 d\nabla^2 S,\end{aligned} \tag{2.3}$$

where

$$\alpha=\frac{r}{\beta},\quad \delta=\frac{\eta}{\beta},\quad \gamma=\frac{\beta L^2}{D_I},\quad d=\frac{D_S}{D_I},\quad \xi_1=\frac{D_1}{D_S},\quad \xi_2=\frac{D_2}{D_S},$$

with $\Omega=1\times 1$, and

$$f(S,I)=\alpha S(1-S)-\frac{SI}{S+I},\qquad g(S,I)=\frac{SI}{S+I}-\delta I.$$

The parameters α and δ are ratios of the growth and death rate to the infection rate, respectively. Meanwhile, parameter γ represents the relative strength of infection [30].

In this study, ξ_2 becomes an important parameter that gives different features. By controlling ξ_2, it means that the infected movement is restricted to the areas with high density of the susceptible. In the case of ξ_2 is zero, i.e., the model without cross-diffusion of the infected term, has been studied by Sun et al. [37]. Furthermore, when ξ_1 and ξ_2 are both zeros then the model returns to the model with self-diffusion case only. Thus, model (2.3) which is proposed in this study is more general since those aforementioned cases are captured by this model.

3. Turing analysis

In the absence of diffusion, model (2.3) has two equilibrium points, $E_0(1,0)$ and $E_1(S_1, I_1)$ with

$$S_1 = \frac{\alpha+\delta-1}{\alpha} \quad \text{and} \quad I_1 = \frac{(1-\delta)(\alpha+\delta-1)}{\alpha\delta}, \tag{3.1}$$

which correspond to the disease-free and endemic equilibrium, respectively. From (3.1), the existence condition of the endemic equilibrium E_1 is $\delta < 1 < \delta + \alpha$. Furthermore, the basic reproduction number is obtained by using the next generation method, namely $R_0 = \frac{1}{\delta}$. Therefore, the existence conditions of E_1 can be expressed as

$$1 < R_0 < 1 + \frac{\alpha}{\delta}.$$

Considering model (2.3), by linearizing near the endemic equilibrium E_1 and setting

$$\mathbf{U} = \begin{pmatrix} u \\ v \end{pmatrix} = \begin{pmatrix} S - S_1 \\ I - I_1 \end{pmatrix},$$

model (2.3) can be expressed as

$$\frac{\partial \mathbf{U}}{\partial t} = \gamma \mathbf{J}\mathbf{U} + \mathbf{D}\nabla^2\mathbf{U},$$

with

$$\mathbf{J} = \begin{pmatrix} f_S(S_1, I_1) & f_I(S_1, I_1) \\ g_S(S_1, I_1) & g_I(S_1, I_1) \end{pmatrix},$$

where $\mathbf{J}$ is the Jacobian matrix and f_S is the partial derivative of function f with respect to S (analogous to others), and the diffusion matrix

$$\mathbf{D} = \begin{pmatrix} d & \xi_1 d \\ -\xi_2 d & 1 \end{pmatrix}.$$

For convenience, the negative sign of ξ_2 is applied in the matrix $\mathbf{D}$ directly. Thus, from now on ξ_2 is taken to be positive in the next calculation. Assume a perturbation near the equilibrium point E_1

$$u \sim \exp(\lambda t)\exp(i\mathbf{k}\cdot\mathbf{r}), \qquad v \sim \exp(\lambda t)\exp(i\mathbf{k}\cdot\mathbf{r}),$$

where λ is the growth rate of the perturbation in time t, i is the imaginary unit with $i^2 = -1$, $\mathbf{k} = (k_x, k_y)$ and $\mathbf{r} = (x, y)$ are the wave number vector and spatial vector in two-dimensional spaces. Note that $k = |\mathbf{k}|$ is the wave number. Substituting $S = S_1 + u$ and $I = I_1 + v$ into model (2.3) and linearizing it by neglecting higher order terms, the characteristic equation is obtained as follows

$$\lambda^2 + a(k^2)\lambda + b(k^2) = 0, \tag{3.2}$$

where

$$\begin{aligned} a(k^2) &= (d+1)k^2 + \mathrm{tr}(\mathbf{J}) = (d+1)k^2 + \gamma(\alpha+\delta-1), \\ b(k^2) &= (\xi_1\xi_2 d^2 + d)k^4 - \gamma(df_I\xi_2 - dg_S\xi_1 + dg_I + f_S)k^2 + \gamma^2|\mathbf{J}|, \end{aligned}$$

$\mathrm{tr}(\mathbf{J})$, $|\mathbf{J}|$ are the trace and determinant of $\mathbf{J}$, respectively.

Proposition 3.1. *Turing instability occurs when the following conditions are satisfied:*

1. $f_S + g_I < 0$;
2. $f_S g_I - f_I g_S > 0$;
3. $df_I\xi_2 - dg_S\xi_1 + dg_I + f_S > 0$;
4. $\frac{(df_I\xi_2 - dg_S\xi_1 + dg_I + f_S)^2}{4d(d\xi_1\xi_2+1)} > |J|$.

The proof of this proposition is given in Appendix A.
Generally, the Turing bifurcation occurs when

$$\mathrm{Im}(\lambda(k)) = 0 \quad \text{and} \quad \mathrm{Re}(\lambda(k)) = 0 \quad \text{at} \quad k = k_c \neq 0. \tag{3.3}$$

By applying conditions (3.3) to the eigenvalues $\lambda(k^2; \alpha, \delta, \gamma, d, \xi_1, \xi_2)$ in (3.2), and fixing other parameters, Turing bifurcation occurs at

$$k_c^2 = \frac{-\gamma\left((\delta^2\xi_1 + \delta^2\xi_2 - \delta^2 - 2\delta\xi_1 + \delta + \xi_1)d - (\delta^2 + \alpha - 1)\right)}{2d(d\xi_1\xi_2 + 1)}, \tag{3.4}$$

with the bifurcation point ξ_2 is

$$\xi_{2,T} = \frac{1}{\delta^3 d}(((\xi_1 - 1)\delta^3 + \delta^2 + (2\alpha - 3)\xi_1\delta - 2(\alpha - 1)\xi_1)d + \delta^3 + \delta(\alpha - 1) + 2\sqrt{H_2}),$$

where

$$H_2 = (\xi_1 - 1)\delta^3 + ((\alpha - 1)\xi_1 - \alpha + 1)\delta^2 + (\alpha - 1)\xi_1\delta + (\alpha - 1)^2\xi_1.$$

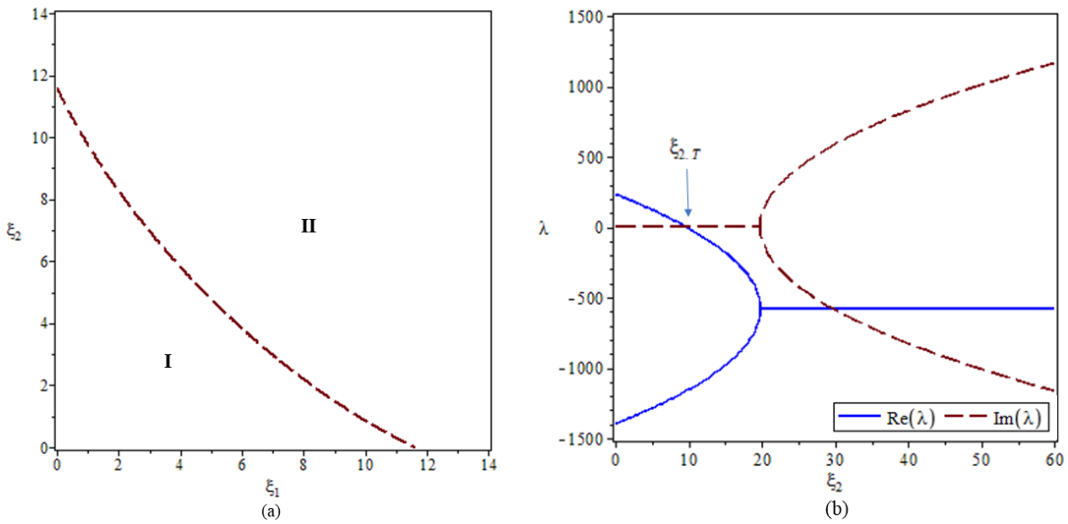

Figure 1: (a) Turing bifurcation diagram of model (2.3). Domain I is the Turing space on ξ_1-ξ_2 plane at $k = k_c$ which is given in (3.4) with $d = 0.05$, $\gamma = 2500$, $\delta = 0.5$, and $\alpha = 0.545$; (b) The eigenvalues of the characteristic correspond to ξ_2 in (a) with $\xi_1 = 1$. The blue-solid and red-dashed show the real and imaginary part of the eigenvalues, respectively.

Turing instability takes place for a pair of (ξ_1, ξ_2) within the Turing space (Domain I) in Figure 1 (a). Under this circumstance, all of the eigenvalues is purely real and one of them must be positive (see Figure 1 (b)). When ξ_2 crosses its bifurcation point $(\xi_{2,T})$ so that (ξ_1, ξ_2) lies on the Domain II, all of the eigenvalues become negative purely real or a pair of complex conjugates with negative real part. As the result, model (2.3) reaches the homogeneous steady state again.

4. The amplitude equations

The study of pattern formation is possible with the help of amplitude equations by using the multiple-scale perturbation analysis [46–49] since close to the onset of Turing bifurcation the dynamics of the system changes very slowly. Let us perturb the endemic equilibrium E_1 by writing $\mathbf{U} = \begin{pmatrix} u \\ v \end{pmatrix}$ with $u = S - S_1, v = I - I_1$, then linearizing model (2.3) near the E_1, we obtain

$$\frac{\partial}{\partial t}\mathbf{U} = \mathbf{L}\mathbf{U} + \frac{1}{2}\begin{pmatrix} f_{uu}u^2 + 2f_{uv}uv + f_{vv}v^2 \\ g_{uu}u^2 + 2g_{uv}uv + g_{vv}v^2 \end{pmatrix} + \frac{1}{6}\begin{pmatrix} f_{uuu}u^3 + 3f_{uuv}u^2v + 3f_{uvv}uv^2 + f_{vvv}v^3 \\ g_{uuu}u^3 + 3g_{uuv}u^2v + 3g_{uvv}uv^2 + g_{vvv}v^3 \end{pmatrix}, \quad (4.1)$$

where $\mathbf{L}$ is a linear operator

$$\mathbf{L} = \begin{pmatrix} a_{11} + d\nabla^2 & a_{12} + d\xi_1\nabla^2 \\ a_{21} - d\xi_2\nabla^2 & a_{22} + \nabla^2 \end{pmatrix}.$$

Choosing ξ_2 as the bifurcation parameter, we analyze the behavior of the controlled parameter close to the onset $\xi_2 = \xi_{2,T}$. Thus, ξ_2 can be expanded in the terms of the small perturbation variable ϵ along with u and v as follows

$$\begin{aligned} \xi_2 &= \xi_{2,T} + \epsilon\xi_{2,1} + \epsilon\xi_{2,2} + \cdots, \\ u &= \epsilon u_1 + \epsilon^2 u_2 + \epsilon^3 u_3 + \cdots, \\ v &= \epsilon v_1 + \epsilon^2 v_2 + \epsilon^3 v_3 + \cdots. \end{aligned} \quad (4.2)$$

Here, ϵ does not have specific physical or biological interpretation. At the same time, the linear operator $\mathbf{L}$ can be also expanded as in the following expression

$$\mathbf{L} = \mathbf{L}_T - \epsilon\begin{pmatrix} 0 & 0 \\ d\nabla^2 & 0 \end{pmatrix}\xi_{2,1} - \epsilon^2\begin{pmatrix} 0 & 0 \\ d\nabla^2 & 0 \end{pmatrix}\xi_{2,2} + \cdots,$$

where

$$\mathbf{L}_T = \begin{pmatrix} a_{11} + d\nabla^2 & a_{12} + d\xi_1\nabla^2 \\ a_{21} - d\xi_{2,T}\nabla^2 & a_{22} + \nabla^2 \end{pmatrix}.$$

The multiple-scale analysis separates the dynamical behavior of the system according to the different time scale or the spatial scale. Here, the time scales are separated as

$$t_0 = t,\ t_1 = \epsilon t, \text{ and } t_2 = \epsilon^2 t, \quad (4.3)$$

which each of the time scales can be considered as independent variables. Therefore, the derivatives with respect to the time are converted to the following terms

$$\frac{\partial}{\partial t} = \frac{\partial}{\partial t_0} + \epsilon\frac{\partial}{\partial t_1} + \epsilon^2\frac{\partial}{\partial t_2} + \cdots.$$

In this present study, the solutions are described by a system of three pairs of active modes $\mathbf{k}_j$ and $-\mathbf{k}_j, j = 1, 2, 3$ with each mode makes angles of $2\pi/3$. Under this circumstance, it satisfies the spatial resonance and $|\mathbf{k}_j| = k_c$ [26, 49]. Thus, at the onset of the Turing instability the solution of model (2.3), $\mathbf{S} = (S, I)$, can be expanded as

$$\mathbf{S} = \mathbf{U}_s + \mathbf{U} = \mathbf{U}_s + \sum_{j=1}^{3} \mathbf{U}_0(A_j \exp(i\mathbf{k}_j \cdot \mathbf{r}) + \overline{A}_j \exp(-i\mathbf{k}_j \cdot \mathbf{r})),$$

where $\mathbf{U}_s = (S_1, I_1)$ is the uniform steady state and $\mathbf{U}_0$ is the eigenvector of the linearized operator $\mathbf{L}$ which defines the direction of the eigenmodes in concentration space (i.e., the ratio of x and y). Meanwhile,

$A_j(t)$ and $\overline{A}_j(t)$ are the perturbation amplitudes associated with a constant wave number $\mathbf{k}_j$ and $-\mathbf{k}_j$, respectively.

The amplitude $A_j(t)$ is a variable that changes slowly with respect to time t. Hence, the derivative with respect to the time t_0 which corresponds to the variable that changes fast does not have an effect on the amplitude A_j [46, 48, 49]. Therefore $\frac{\partial}{\partial t_0} = 0$ so that

$$\frac{\partial A_j}{\partial t} = \epsilon \frac{\partial A_j}{\partial t_1} + \epsilon^2 \frac{\partial A_j}{\partial t_2} + \cdots . \tag{4.4}$$

Up to the third order in perturbation, the spatiotemporal evolution of the amplitudes $A_j(t)$ are described by the following form

$$\tau_0 \frac{\partial A_j}{\partial t} = \mu A_j + q_0 \overline{A}_\kappa \overline{A}_\ell - (q_1 |A_j|^2 + q_2(|A_\kappa|^2 + |A_\ell|^2))A_j, \;\; j \neq \kappa \neq \ell, j = 1,2,3, \tag{4.5}$$

in which $\mu = \frac{\xi_{2,T} - \xi_2}{\xi_{2,T}}$ is a normalized distance to onset. The form of (4.5) is general form for Turing bifurcation, but the exact expressions of the coefficients are specific to the model [41, 45]. By further calculations, the exact expressions of the coefficients for model (2.3) are given as

$$\tau_0 = \frac{f+g}{k_c^2 g f d \xi_{2,T}}, \quad q_0 = \frac{g g_2 + f_2}{k_c^2 g f d \xi_{2,T}}, \quad q_1 = -\frac{G_1}{k_c^2 g f d \xi_{2,T}}, \quad q_2 = -\frac{G_2}{k_c^2 g f d \xi_{2,T}}.$$

Detailed calculation of the parameters can be found in Appendix B.

4.1. The amplitude stability

Assume that each of the amplitude equations may be expressed into a polar coordinate $A_j(t) = \rho_j(t)\exp(i\phi_j(t))$, where $\rho_j = |A_j|$ and ϕ_j represent the mode and corresponding phase angle, respectively. Substituting $A_j(t)$ into the amplitude equations (4.5) and separating the real and imaginary parts yield

$$\tau_0 \frac{\partial \phi}{\partial t} = -q_0 \frac{\rho_1^2\rho_2^2 + \rho_2^2\rho_3^2 + \rho_2^2\rho_3^2}{\rho_1\rho_2\rho_3} \sin\phi, \tag{4.6}$$

$$\tau_0 \frac{\partial \rho_j}{\partial t} = \mu\rho_j + q_0\rho_\kappa\rho_\ell \cos\phi - q_1\rho_j^3 - q_2(\rho_\kappa^2 + \rho_\ell^2)\rho_j, \tag{4.7}$$

for $j = 1,2,3$, with $j \neq \kappa \neq \ell$ and $\phi = \phi_1 + \phi_2 + \phi_3$. From Equation (4.6), we obtain the stable solutions which are given by $\phi = 0$ with $q_0 > 0$ or $\phi = \pi$ with $q_0 < 0$. Applying these values and using the linear stability analysis, the dynamical system (4.7) has the following solutions [10, 29, 42].

1. The stable homogeneous solution, $\rho_1 = \rho_2 = \rho_3 = 0$, occurs if $\mu < \mu_2 = 0$. In other words, the spatial pattern occurs if it is unstable, i.e., when $\mu > \mu_2 = 0$.
2. The stripes are given by
$$\rho_1 = \sqrt{\frac{\mu}{q_1}}, \rho_2 = \rho_3 = 0,$$
and it is stable if $\mu > \mu_3 = \frac{q_0^2 q_1}{(q_1 - q_2)^2}$ and unstable if $\mu < \mu_3$.
3. The hexagonal is given by $\rho_1 = \rho_2 = \rho_3 = \rho$, that is
$$\rho = \frac{|q_0| \pm \sqrt{q_0^2 + 4(q_1 + 2q_2)\mu}}{2(q_1 + 2q_2)},$$
and exist when $\mu > \mu_1 = -\frac{q_0^2}{4(q_1+2q_2)}$. The solution
$$\rho = \frac{|q_0| + \sqrt{q_0^2 + 4(q_1 + 2q_2)\mu}}{2(q_1 + 2q_2)}$$
is stable if $\mu < \mu_4 = \frac{q_0^2(2q_1+q_2)}{(q_1-q_2)^2}$, and otherwise unstable.

4. The mixed states are given by

$$\rho_1 = \frac{|q_0|}{q_2 - q_1}, \rho_2 = \rho_3 = \sqrt{\frac{\mu - q_1\rho_1^2}{q_1 + q_2}},$$

with $\mu > q_1\rho_1^2$ which is always unstable.

5. Pattern selection

5.1. Numerical method

In this section, model (2.3) is solved numerically to confirm the theoretical analysis by discretizing the space and time of the model. In practice, the continuous problem defined by a reaction-diffusion system in two-dimensional is solved in a discrete domain with $M \times N$ lattice sites. In the discrete system the Laplacian describing diffusion is calculated using finite differences, i.e., the derivatives are approximated by differences over $\triangle h$ which approach the derivative for $\triangle h \to 0$. Meanwhile, the time evolution is discretized with the step size $\triangle t$ and can be solved by using the Euler method. It means that the approximation of the next time step concentration value based on the change rate of the previous time step concentration. Without losing of generality, it is also assumed that $\partial\Omega \in \mathbf{C}^2$. In the present study, model (2.3) is solved with a positive initial values near E_1 with the small random perturbation and boundary condition (2.2) with $\triangle h = 0.01, \triangle t = 1 \times 10^{-5}$ in a system size 1×1. We perform extensive numerical simulations by varying the values of ξ_2 within the Turing space in Figure 1 (a). The simulations are terminated until they show a behavior that does not experience the change its characteristics anymore.

5.2. The numerical vs the amplitude analysis

From a series of numerical simulations, there are five types of pattern discovered from the model, namely the spots, spots-stripes, stripes, stripes-holes, and holes (Figure 2 (a)-(e), respectively). Compared with the results of Sun et al. [37], the addition of cross-diffusion of infected term to the model [37] revealed a richer type of pattern. The model in [37] only revealed two types of patterns, namely the spots-stripes and stripes. In compliance with other results of the spatial epidemic models [5, 12, 24, 35, 37, 40, 44], we also discover that the density distribution of the susceptible and infected always reveal the same patterns with positive correlation. It indicates that the densities of the susceptible and infected move in tandem in the same direction. Therefore, only the patterns of the infected are shown.

According to the amplitude stability analysis in the previous section, variation of μ is responsible for the emergence of various patterns which is controlled by the cross-diffusion coefficient of the infected, ξ_2. Upon further calculations, with the set of parameters $\alpha = 0.545, \delta = 0.5, \gamma = 2500, d = 0.05$, and $\xi_1 = 1$, it yields $\mu_1 = -2.121\text{x}10^{-8}$, $\mu_2 = 0, \mu_3 = 0.0547$, and $\mu_4 = 0.164$. When the value of ξ_2 increases, a sequence of patterns is performed by the model, i.e., the spots$\to$ spots-stripes $\to$ stripes $\to$ stripes-holes $\to$ holes.

In relation to the theoretical analysis, the μ of the spots, spots-stripes and stripes (Figures 2 (a)-(c)) are $0.9989, 0.6929, 0.2835$ which are bigger than μ_4. These simulations are not in accordance with the theoretical results. The amplitude equations fail to explain the situation. However, the stripes-holes in Figure 2 (d) ($\xi_2 = 8.5$) satisfies $\mu_3 < \mu = 0.13001 < \mu_4$ which according to the theoretical analysis performs the mixture of stripes and holes. That is to say, the numerical simulation is in accordance with the amplitude analysis. Moreover, the holes in Figure 2 (e) ($\xi_2 = 9.5$) are also validated by the theoretical analysis since it satisfies $\mu_2 < \mu = 0.0276 < \mu_3$.

When ξ_2 gets very close to its bifurcation point, the μ always satisfies $\mu_2 < \mu < \mu_3$ so that the model reveals the holes but it comes very slowly. Meanwhile, if $\xi_2 > \xi_{2,T}$, the solution of the system returns to the homogeneous steady state, E_1. Under this circumstance, the $\mu < \mu_2$, therefore the solution becomes stable and shows no pattern. This simulation result is also in accordance with the theoretical analysis.

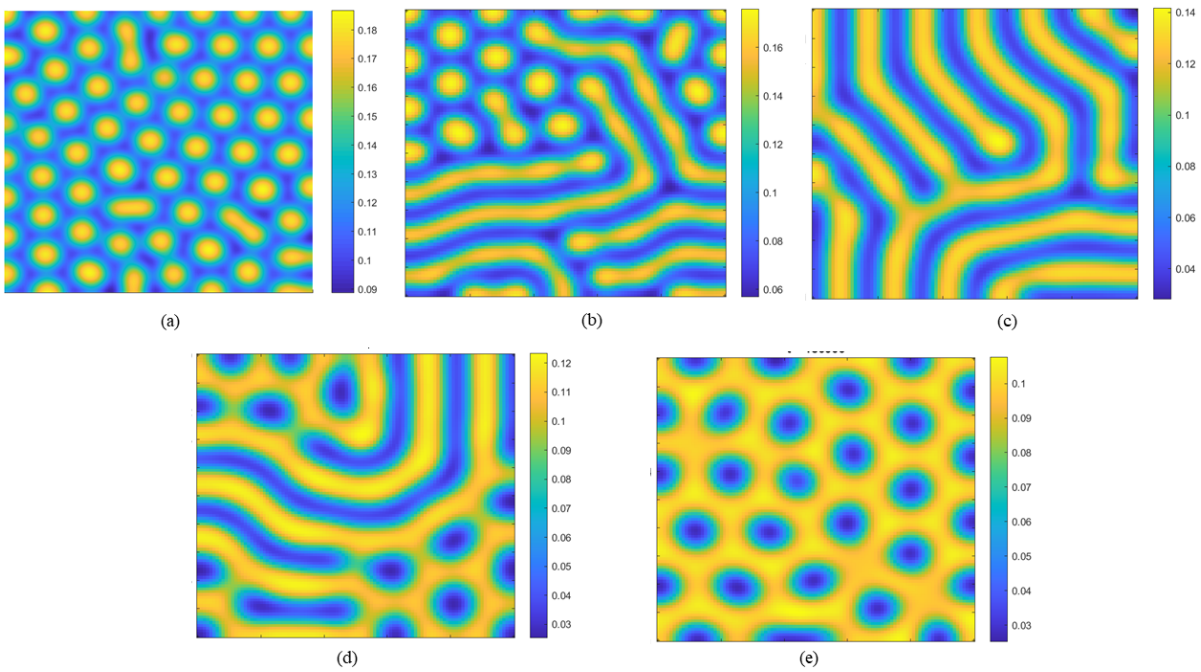

Figure 2: Patterns of the infected of model (2.3) where $d = 0.05, \gamma = 2500, \delta = 0.5, \alpha = 0.545$, $\xi_1 = 1$ with various values of ξ_2. (a) $\xi_2 = 0.01$, (b) $\xi_2 = 3$, (c) $\xi_2 = 7$, (d) $\xi_2 = 8.5$, (e) $\xi_2 = 9.5$.

5.3. The biological interpretation

In this subsection, we provide the biological interpretation of the five patterns of the model. In Figures 3-7, we show the examples of pattern formations by time evolution for each pattern. The spots (Figure 3), represented by the yellow hexagons on a blue background, indicate that the high density of the infected occurs only in certain areas, with almost no infection (or very low) at the rest of the region. This pattern is obtained when small values are given to ξ_2 which means that the infected has limited access to higher density areas of the susceptible. From an epidemiological point of view, the region is safe from a disease outbreak.

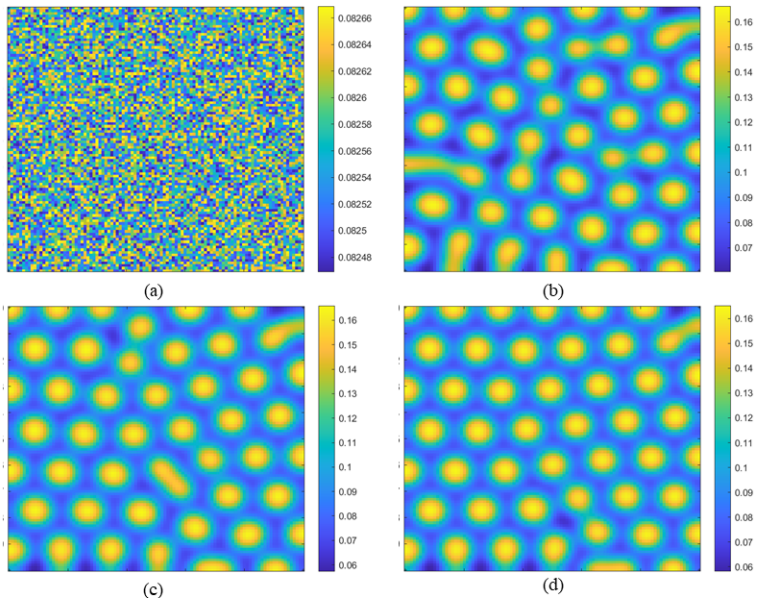

Figure 3: The spots of the infected of model (2.3) by the time evolution with $d = 0.05, \gamma = 2500, \alpha = 0.545, \delta = 0.5, \xi_1 = 1$, and $\xi_2 = 0.01$.

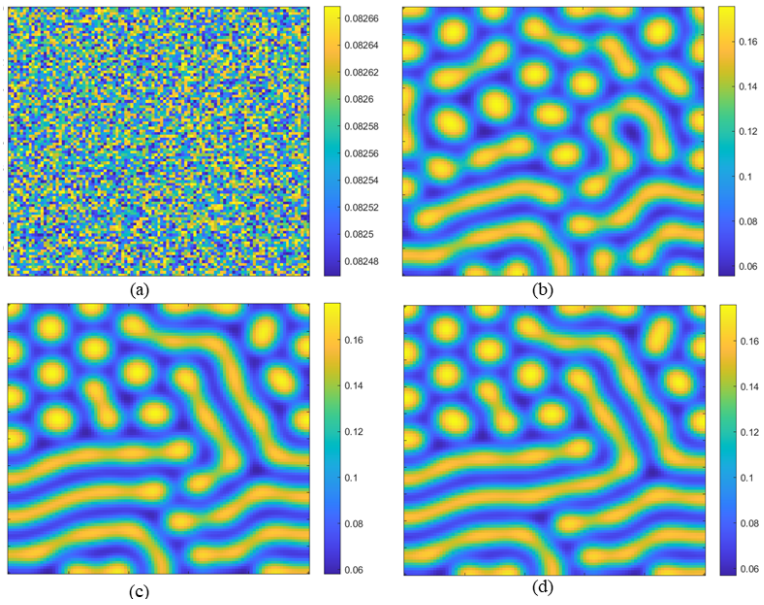

Figure 4: The spots-stripes of the infected of model (2.3) by the time evolution with $d = 0.05, \gamma = 2500, \alpha = 0.545, \delta = 0.5, \xi_1 = 1$, and $\xi_2 = 3$.

Once the value of ξ_2 increases, some spots will unite forming the stripes and will show the spots-stripes as in Figure 4. This indicates that areas nearby the spots begin to incrementally increase the density of the infected. The higher the movement of the infected to areas with the high density of the susceptible, the more new infections occur in the new places, as it can be seen in Figure 5 where all the spots merge each other forming the stripes. This situation indicates that disease starts to spread over to wider areas.

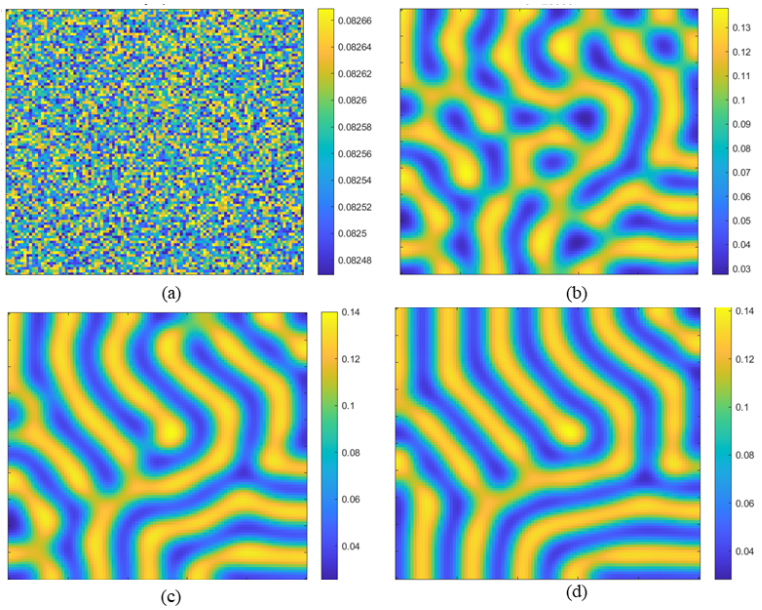

Figure 5: The stripes of the infected of model (2.3) by the time evolution with $d = 0.05, \gamma = 2500, \alpha = 0.545, \delta = 0.5, \xi_1 = 1$, and $\xi_2 = 7$.

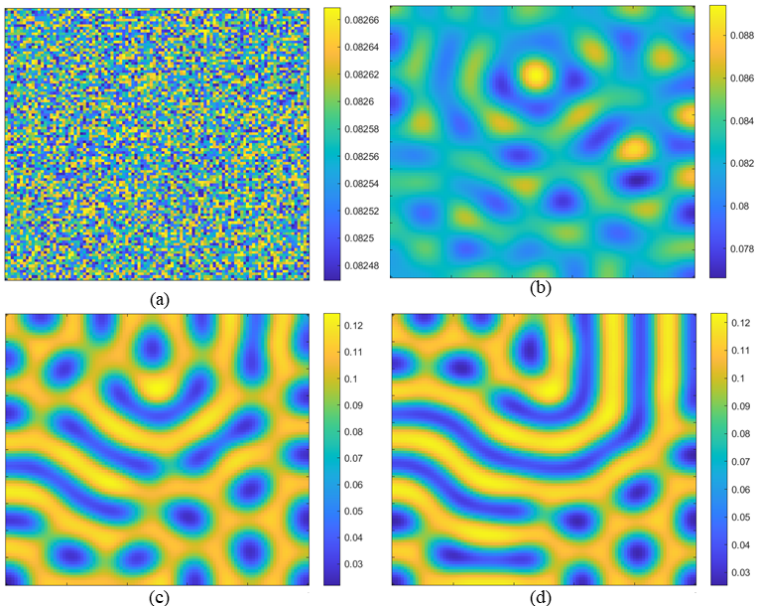

Figure 6: The stripes-holes of the infected of model (2.3) by the time evolution with $d = 0.05, \gamma = 2500, \alpha = 0.545, \delta = 0.5, \xi_1 = 1$, and $\xi_2 = 8.5$.

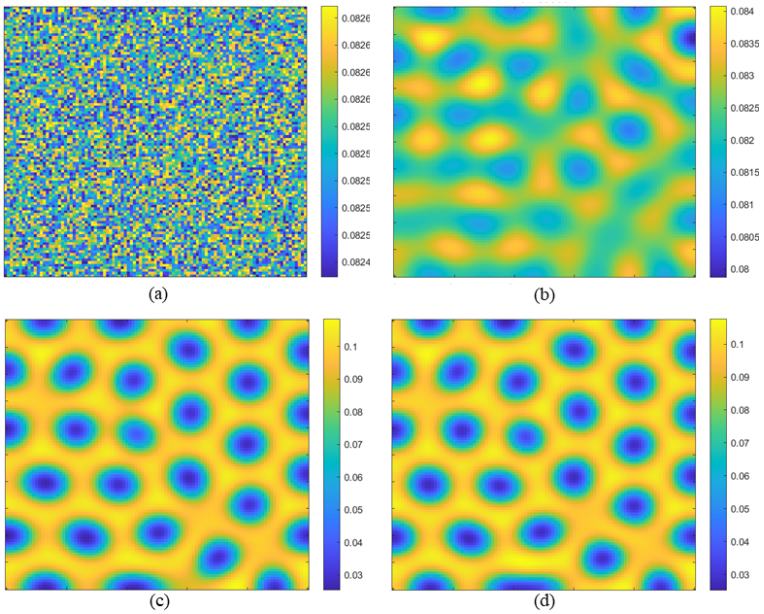

Figure 7: The holes of the infected of model (2.3) by the time evolution with $d = 0.05, \gamma = 2500, \alpha = 0.545, \delta = 0.5, \xi_1 = 1$, and $\xi_2 = 9.5$.

Meanwhile, the stripes-holes (Figure 6) show a worse situation than the three previous patterns, since it describes a region that starts to experience an outbreak in many areas. This pattern is obtained when the value of ξ_2 is greater than the ξ_2 value of the previous patterns, which means that the infected moves to areas with a higher density of the susceptible faster than before.

Finally, when ξ_2 gets bigger, then the model shows the holes. This pattern is dominated by the yellow color in a spatial domain, which indicates that a high density of infected occurs in many areas in a region, although there are some places that have a low density of the infected. Thus, from an epidemiological point of view, the holes like in Figure 7 show the worst situation and indicate that a disease outbreak may occur in a region [40, 42].

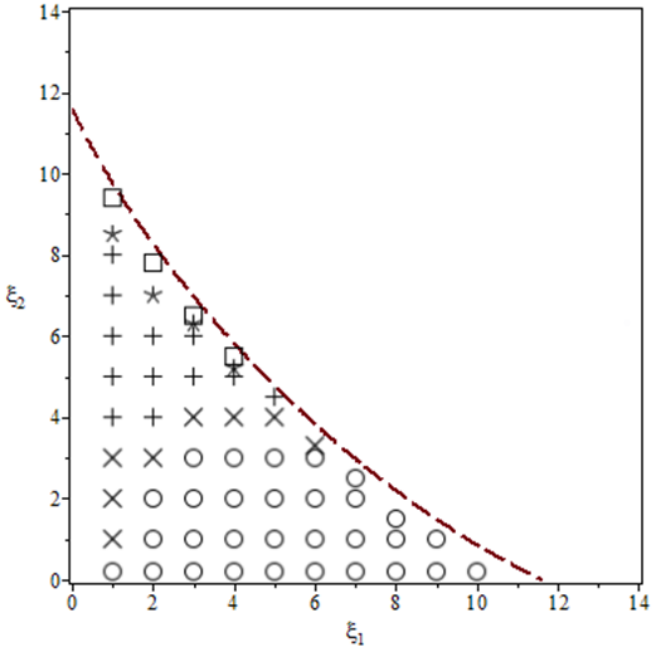

Figure 8: The emergence location of the five typical patterns of model (2.3) within the Turing space with parameters $\gamma = 2500, d = 0.05, \alpha = 0.545, \delta = 0.5$. The signs $\circ, \times, +, \star$, and $\square$ correspond to the spots, spots-stripes, stripes, stripes-holes, and holes, respectively.

The emergence location for all possible patterns related to variation of ξ_1 and ξ_2 within the Turing space are shown in Figure 8 which the signs $\circ, \times, +, \star$, and $\square$ refer to the spots, spots-stripes, stripes, stripes-holes, and holes, respectively. From Figure 8 we can observe that the holes revealed by the model if the value of ξ_2 are quite large. This means that infected people are allowed to move freely, especially to areas of high density of the susceptible. Outbreaks can be prevented by controlling the movement of the infected by setting a smaller value to ξ_2 in the model. In this state, the pattern turns into the stripes-holes, stripes, spots-stripes, and even the spots. Furthermore, if the value of ξ_1 increases, then the model reveals a pattern that indicates a better situation.

6. Conclusions

In this study, we consider and analyze a spatial epidemic model with cross-diffusion of the susceptible and infected simultaneously under zero-flux boundary condition. The spatial pattern induced by cross-diffusion was investigated analytically and numerically. First, we derived Turing instability conditions for the model and Turing space corresponding to the bifurcation parameter, i.e, infected cross-diffusion coefficient. Multiple scale analysis is used to derive the amplitude equations. From stability analysis of the amplitude equations, the types of Turing pattern which emerge near the Turing bifurcation threshold are found. Besides, an extensive numerical simulation was carried out to validate the analytic results and revealed five types of patterns. Comparing to the results of Sun et al. in [37], the constructed model in this study reveals richer patterns, not only the stripe and spots-stripes. The five patterns are the spots, spots-stripes, stripes, stripes-holes, and holes. It means that the model shows more complex densities distribution of the population spatially. Furthermore, analytic and numerical results are in compliance when bifurcation parameter value near to the Turing bifurcation threshold.

On the other hand, we focus on the competition effects of cross-diffusion coefficients of the susceptible and infected. If the cross-diffusion coefficient of the infected is much bigger than the susceptible, then it may trigger the outbreak. That is to say, the infected moves faster to the areas with a high density of the susceptible than susceptible stays away from the infected. Hence, this study shows further results, i.e.,

cross-diffusion of the infected in this model confirms the importance of controlling the infected movement to prevent the spread of an infectious disease to a wider area.

Nowadays, people all over the world are facing an infectious disease caused by the Coronavirus, which has spread in many countries. In addition to medical treatment such as vaccines, restrictions on the movement of infected people need to be carried out to prevent the spread of infectious diseases. Local governments can issue restrictions on the movement of the infected especially to areas with high density of the susceptible, such as self-quarantine or travel bans to other areas until they recover. In addition, the cross-diffusion of the susceptible shows that when they have the awareness to stay away from the infected, it is very helpful in breaking the chain of disease transmission. In this study, we chose India and Japan as the samples, since those countries had been struck repeatedly from wave to wave.

Hopefully, the method and results will provide a contribution to enriching the study of pattern formations in the spatial epidemic model, also as a basis for decision-making.

Acknowledgment

The authors are grateful to the editors and anonymous referees for their comments and suggestions which improved the presentation of the manuscript. This research was supported by the Indonesian Education Scholarship Program, Ministry of Finance and Research, Technology and Higher Education of the Republic of Indonesia (No.PRJ-144/LPDP.4/2019). The author also thanks Prof. Hadi Susanto for fruitful suggestions.

Appendix A

Proof. In the absence of diffusion, in order to guarantee the stability, all of the eigenvalues of the Jacobian matrix corresponding to E_1 must be negative. This implies that the trace $\mathrm{tr}(\mathbf{J}) < 0$ and determinant $|\mathbf{J}| > 0$. Thus

$$f_S + g_I < 0, \quad \text{and} \quad f_S g_I - f_I g_S > 0. \tag{6.1}$$

Turing instability occurs if E_1 is linearly stable in the absence of the spatial variable but becomes unstable in the presence of diffusion [30]. If the real part of the eigenvalues $\mathrm{Re}(\lambda(k^2)) > 0$ for some $k^2 \neq 0$, then the instability occurs [9]. Equation (6.1) guarantees that $a(k^2)$ is positive, then the only possibility to obtain $\mathrm{Re}(\lambda(k^2)) > 0$ for some $k^2 \neq 0$ is if $b(k^2) < 0$. Therefore, the necessary condition is if

$$df_I\xi_2 - dg_S\xi_1 + dg_I + f_S > 0, \tag{6.2}$$

but not sufficient to obtain $\mathrm{Re}(\lambda(k^2)) > 0$. The minimum value of $b(k^2)$ is

$$b(k^2)_{\min} = \gamma^2\left(|\mathbf{J}| - \frac{(df_I\xi_2 - dg_S\xi_1 + dg_I + f_S)^2}{4d(d\xi_1\xi_2 + 1)}\right), \tag{6.3}$$

when

$$k^2_{\min} = \gamma\frac{(df_I\xi_2 - dg_S\xi_1 + dg_I + f_S)}{2d(d\xi_1\xi_2 + 1)}.$$

Thus, the sufficient condition to obtain $b(k^2) < 0$ for some $k^2 \neq 0$ is

$$\frac{(df_I\xi_2 - dg_S\xi_1 + dg_I + f_S)^2}{4d(d\xi_1\xi_2 + 1)} > |\mathbf{J}|. \tag{6.4}$$

Equations (6.1), (6.2), and (6.4) prove the Proposition 3.1. □

Appendix B

Substituting (4.2) and (4.3) into (4.1) and equating the coefficients of ϵ, ϵ^2, and ϵ^3, these three following expressions are obtained

$$\mathcal{O}(\epsilon) : \mathbf{L}_T \begin{pmatrix} u_1 \\ v_1 \end{pmatrix} = 0, \tag{6.5}$$

$$\begin{aligned} \mathcal{O}(\epsilon^2) : \mathbf{L}_T \begin{pmatrix} u_2 \\ v_2 \end{pmatrix} &= \frac{\partial}{\partial t_1} \begin{pmatrix} u_1 \\ v_1 \end{pmatrix} + \xi_{2,1} \begin{pmatrix} 0 & 0 \\ d & 0 \end{pmatrix} \nabla^2 \begin{pmatrix} u_1 \\ v_1 \end{pmatrix} - \frac{1}{2} \begin{pmatrix} f_{uu}u_1^2 + 2f_{uv}u_1v_1 + f_{vv}v_1^2 \\ g_{uu}u_1^2 + 2g_{uv}u_1v_1 + g_{vv}v_1^2 \end{pmatrix} \\ &= \begin{pmatrix} F_x \\ F_y \end{pmatrix}, \end{aligned} \tag{6.6}$$

$$\mathcal{O}(\epsilon^3) : \mathbf{L}_T \begin{pmatrix} u_3 \\ v_3 \end{pmatrix} = \begin{pmatrix} G_x \\ G_y \end{pmatrix}, \tag{6.7}$$

where

$$\begin{aligned} \begin{pmatrix} G_x \\ G_y \end{pmatrix} &= \begin{pmatrix} \frac{\partial u_2}{\partial t_1} + \frac{\partial u_1}{\partial t_2} \\ \frac{\partial v_2}{\partial t_1} + \frac{\partial v_1}{\partial t_2} \end{pmatrix} + \xi_{2,1} \begin{pmatrix} 0 & 0 \\ d & 0 \end{pmatrix} \nabla^2 \begin{pmatrix} u_2 \\ v_2 \end{pmatrix} + \xi_{2,2} \begin{pmatrix} 0 & 0 \\ d & 0 \end{pmatrix} \nabla^2 \begin{pmatrix} u_1 \\ v_1 \end{pmatrix} \\ &- \begin{pmatrix} f_{uu}u_1u_2 + f_{uv}(u_1v_2 + u_2v_1) + f_{vv}v_1v_2 \\ g_{uu}u_1u_2 + g_{uv}(u_1v_2 + u_2v_1) + g_{vv}v_1v_2 \end{pmatrix} \\ &- \frac{1}{6} \begin{pmatrix} f_{uuu}u_1^3 + 3f_{uuv}u_1^2v_1 + 3f_{uvv}u_1v_1^2 + f_{vvv}v_1^3 \\ g_{uuu}u_1^3 + 3g_{uuv}u_1^2v_1 + 3g_{uvv}u_1v_1^2 + g_{vvv}v_1^3 \end{pmatrix}. \end{aligned} \tag{6.8}$$

Firstly, at $\mathcal{O}(\epsilon)$ we have a linear system (6.5). Since $\mathbf{L}_T$ is the linear operator of the system at the Turing bifurcation threshold, then $\begin{pmatrix} u_1 \\ v_1 \end{pmatrix}$ is a linear combination of the eigenvectors corresponding to the eigenvalue zero. Let

$$\begin{pmatrix} u_1 \\ v_1 \end{pmatrix} = \begin{pmatrix} U_j \\ V_j \end{pmatrix} \left(\sum_{j=1}^{3} \exp(i\mathbf{k}_j \cdot \mathbf{r}) \right) + \text{c.c.},$$

with c.c. is the complex conjugate term. By solving (6.5) we obtain $U_j = fV_j$ so

$$\begin{pmatrix} u_1 \\ v_1 \end{pmatrix} = \begin{pmatrix} f \\ 1 \end{pmatrix} \left(\sum_{j=1}^{3} W_j \exp(i\mathbf{k}_j \cdot \mathbf{r}) \right) + \text{c.c.}, \tag{6.9}$$

where W_j is the amplitude of the mode $\exp(i\mathbf{k}_j \cdot \mathbf{r})$ under the first perturbation with $j = 1, 2, 3$, $|\mathbf{k}_j| = k_c$ and

$$f = \frac{k_c^2 - a_{22}}{a_{21} + k_c^2 d\xi_{2,T}}.$$

Secondly, at $\mathcal{O}(\epsilon^2)$, the solution of Equation (6.6) can be expanded into the form

$$\begin{aligned} \begin{pmatrix} u_2 \\ v_2 \end{pmatrix} &= \begin{pmatrix} X_0 \\ Y_0 \end{pmatrix} + \sum_{j=1}^{3} \left(\begin{pmatrix} X_j \\ Y_j \end{pmatrix} \exp(i\mathbf{k}_j \cdot \mathbf{r}) + \begin{pmatrix} X_{jj} \\ Y_{jj} \end{pmatrix} \exp(2i\mathbf{k}_j \cdot \mathbf{r}) \right) \\ &+ \begin{pmatrix} X_{12} \\ Y_{12} \end{pmatrix} \exp(i(\mathbf{k}_1 - \mathbf{k}_2) \cdot \mathbf{r}) + \begin{pmatrix} X_{23} \\ Y_{23} \end{pmatrix} \exp(i(\mathbf{k}_2 - \mathbf{k}_3) \cdot \mathbf{r}) \\ &+ \begin{pmatrix} X_{31} \\ Y_{31} \end{pmatrix} \exp(i(\mathbf{k}_3 - \mathbf{k}_1) \cdot \mathbf{r}) + \text{c.c.}. \end{aligned} \tag{6.10}$$

Let $\mathbf{L}_T^+$ be the adjoint operator of $\mathbf{L}_T$. According to the Fredholm solvability condition, the vector function of the right-hand side (RHS) of (6.6) must be orthogonal to the eigenvectors of the zero eigenvalue of $\mathbf{L}_T^+$ to ensure the nontrivial solution of this equation. The eigenvectors of the operator $\mathbf{L}_T^+$ are

$$\begin{pmatrix} 1 \\ g \end{pmatrix} \exp(i\mathbf{k}_j \cdot \mathbf{r}) + \text{c.c.},$$

for $j = 1, 2, 3$ with

$$g = \frac{a_{11} - dk_c^2}{a_{21} + dk_c^2 \xi_{2,T}}.$$

The orthogonality condition is

$$(1, g) \begin{pmatrix} F_x^j \\ F_y^J \end{pmatrix} = 0,$$

where F_x^j and F_y^J are the coefficients of $\exp(i\mathbf{k}_j \cdot \mathbf{r})$ term in F_x and F_y. For instance, substituting (6.9) to (6.6) yields

$$\begin{pmatrix} F_x^1 \\ F_x^1 \end{pmatrix} = \begin{pmatrix} f \\ 1 \end{pmatrix} \frac{\partial W_1}{\partial t_1} + \xi_{2,1} \begin{pmatrix} 0 & 0 \\ d & 0 \end{pmatrix} (-k_c^2) \begin{pmatrix} f \\ 1 \end{pmatrix} W_1 - \begin{pmatrix} f_2 \\ g_2 \end{pmatrix} \overline{W}_2 \overline{W}_3$$

with

$$\begin{pmatrix} f_2 \\ g_2 \end{pmatrix} = \begin{pmatrix} f_{uu} f^2 + 2 f_{uv} f + f_{vv} \\ g_{uu} f^2 + 2 g_{uv} f + g_{vv} \end{pmatrix}.$$

Using the solvability condition, the following relations are obtained

$$\begin{aligned} (f + g) \frac{\partial W_1}{\partial t_1} &= k_c^2 df g \xi_{2,1} W_1 + (f_2 + g g_2) \overline{W}_2 \overline{W}_3, \\ (f + g) \frac{\partial W_2}{\partial t_1} &= k_c^2 df g \xi_{2,1} W_2 + (f_2 + g g_2) \overline{W}_3 \overline{W}_1, \\ (f + g) \frac{\partial W_3}{\partial t_1} &= k_c^2 df g \xi_{2,1} W_3 + (f_2 + g g_2) \overline{W}_1 \overline{W}_2. \end{aligned} \tag{6.11}$$

Substituting (6.10) into (6.6) and collecting the coefficients of $\exp(i\mathbf{k}_j \cdot \mathbf{r})$ and so on, yields following results

$$\begin{pmatrix} X_0 \\ Y_0 \end{pmatrix} = \begin{pmatrix} z_{x0} \\ z_{y0} \end{pmatrix} (|W|_1^2 + |W|_2^2 + |W|_3^2), \qquad X_j = f Y_j,$$

$$\begin{pmatrix} X_{jj} \\ Y_{jj} \end{pmatrix} = \begin{pmatrix} z_{x1} \\ z_{y1} \end{pmatrix} W_j^2, \qquad \begin{pmatrix} X_{12} \\ Y_{12} \end{pmatrix} = \begin{pmatrix} z_{x2} \\ z_{y2} \end{pmatrix} W_1^2 \overline{W}_2,$$

$$\begin{pmatrix} X_{23} \\ Y_{23} \end{pmatrix} = \begin{pmatrix} z_{x2} \\ z_{y2} \end{pmatrix} W_2^2 \overline{W}_3, \qquad \begin{pmatrix} X_{31} \\ Y_{31} \end{pmatrix} = \begin{pmatrix} z_{x2} \\ z_{y2} \end{pmatrix} W_3^2 \overline{W}_1.$$

Lastly, at $\mathcal{O}(\epsilon^3)$ we have Equation (6.7). Collecting the coefficients for $\exp(i\mathbf{k}_1 \cdot \mathbf{r})$ from (6.8), namely $\begin{pmatrix} G_x^1 \\ G_y^1 \end{pmatrix}$, and using the Fredholm solvability condition as in $\mathcal{O}(\epsilon^2)$ case, we obtain

$$(1, g) \begin{pmatrix} G_x^1 \\ G_y^1 \end{pmatrix} = 0,$$

and

$$\begin{aligned} (f + g) \left(\frac{\partial W_1}{\partial t_2} + \frac{\partial Y_1}{\partial t_1} \right) &= g f d k_c^2 (\xi_{2,1} Y_1 + \xi_{2,2} W_1) + (g g_2 + f_2)(\overline{Y}_2 \overline{W}_3 + \overline{Y}_3 \overline{W}_2) \\ &\quad + (G_1 |W_1|^2 + G_2 (|W_2|^2 + |W_3|^2) W_1), \end{aligned} \tag{6.12}$$

here

$$
\begin{aligned}
f_3 &= f_{uuu}f^3 + 3f_{uuv}f^2 + 3f_{uvv}f + f_{vvv},\\
g_3 &= g_{uuu}f^3 + 3g_{uuv}f^2 + 3g_{uvv}f + g_{vvv},\\
h_1 &= (g_{uu}g + f_{uu})f + g_{uv}g + f_{uv},\\
h_2 &= (g_{uv}g + f_{uv})f + g_{vv}g + f_{vv},\\
G_1 &= (z_{xo} + z_{x1})h_1 + (z_{yo} + z_{y1})h_2 + \frac{1}{2}(gg_3 + f_3),\\
G_2 &= (z_{xo} + z_{x2})h_1 + (z_{yo} + z_{y2})h_2 + (gg_3 + f_3).
\end{aligned}
$$

The terms of $\left(\frac{\partial W_2}{\partial t_2} + \frac{\partial Y_2}{\partial t_1}\right)$ and $\left(\frac{\partial W_3}{\partial t_2} + \frac{\partial Y_3}{\partial t_1}\right)$ can be obtained by permutation of the subscript of W as well. Considering equation (4.4), the amplitude equations $A_j(t)$ can be expanded as

$$A_j(t) = \epsilon W_j(t) + \epsilon^2 Y_j(t) + \cdots. \tag{6.13}$$

Substituting (6.13) to (4.4) and using the solvability conditions (6.11) and (6.12), the amplitude equations corresponding to $A_j(t)$ for $j = 1, 2, 3$ is derived as given in (4.5).

References

[1] W. Abid, R. Yafia, M. Aziz-Alaoui, A. Aghriche, *Turing instability and hopf bifurcation in a modified leslie-gower predator-prey model with cross-diffusion*, Int. J. Bifurc. Chaos, **28** (2018), 17 pages.

[2] L. J. S. Allen, B. M. Bolker, Y. Lou, A. L. Nevai, *Asymptotic profiles of the steady states for an sis epidemic reaction-diffusion model*, Disc. Cont. Dyn. Syst., **21** (2008), 1–20.

[3] M. Banerjee, S. Ghorai, N. Mukherjee, *Study of cross-diffusion induced turing patterns in a ratio-dependent prey-predator model via amplitude equations*, Appl. Math. Model., **55** (2018), 383–399.

[4] S. Berres, J. G. Marin, *On epidemics models with nonlinear cross diffusion*, 20th International Congress on Modelling and Simulation, (2013).

[5] Y. L. Cai, D. X. Chi, W. B. Liu, W. M. Wang, *Stationary patterns of a cross-diffusion epidemic model*, Abstr. Appl. Anal., **2013** (2013), 10 pages.

[6] Y. L. Cai, S. L. Yan, H. L. Wang, X. Z. Lian, W. M. Wang, *Spatiotemporal dynamics in a reaction-diffusion epidemic model with a time-delay in transmission*, Internat. J. Bifur. Chaos Appl. Sci. Engrg., **25** (2015), 16 pages.

[7] V. Castets, E. Dulos, J. Boissonade, P. De Kepper, *Experimental evidence of a sustained standing turing-type nonequilibrium chemical pattern*, Phys. Rev. Lett., **64** (1990), 11 pages.

[8] M. Chen, R. Wu, B. Liu, L. Chen, *Pattern selection in a predator-prey model with michaelis-menten type nonlinear predator harvesting*, Ecol. Complex., **36** (2018), 239–249.

[9] J. M. Chung, E. Peacock-Lopez, *Bifurcation diagrams and turing patterns in a chemical self-replicating reaction-diffusion system with cross diffusion*, J. Chem. Phys., **127** (2007), p. 174903.

[10] S. Ciliberto, P. Coullet, J. Lega, E. Pampaloni, C. Perez-Garcia, *Defects in roll-hexagon competition*, Phys. Rev. Lett., **65** (1990), 10 pages.

[11] M. C. Cross, P. C. Hohenberg, *Pattern formation outside of equilibrium*, Rev. Mod. Phys., **65** (1993), 9 pages.

[12] Y. Fan, *Pattern formation of an epidemic model with cross diffusion*, Appl. Math. Comput., **228** (2014), 311–319.

[13] G. Gambino, M. Lombardo, S. Lupo, M. Sammartino, *Super-critical and sub-critical bifurcations in a reaction-diffusion schnakenberg model with linear cross-diffusion*, Ric. Mat., **65** (2016), 449–467.

[14] S. Ghorai, S. Poria, *Turing patterns induced by cross-diffusion in a predator-prey system in presence of habitat complexity*, Chaos Solitons Fractals, **91** (2016), 421–429.

[15] L. N. Guin, *Existence of spatial patterns in a predator-prey model with self-and cross-diffusion*, Appl. Math. Comput., **226** (2014), 320–335.

[16] L. N. Guin, S. Acharya, *Dynamic behaviour of a reaction-diffusion predator-prey model with both refuge and harvesting*, Nonlinear Dyn., **88** (2017), 1501–1533.

[17] L. N. Guin, M. Haque, P. K. Mandal, *The spatial patterns through diffusion-driven instability in a predator-prey model*, Appl. Math. Model., **36** (2012), 1825–1841.

[18] L. N. Guin, P. K. Mandal, *Effect of prey refuge on spatiotemporal dynamics of the reaction-diffusion system*, Comput. Math. with Appl., **68** (2014), 1325–1340.

[19] R. Han, L. N. Guin, B. Dai, *Cross-diffusion-driven pattern formation and selection in a modified leslie-gower predator-prey model with fear effect*, J. Biol. Syst., **28** (2020), 27–64.

[20] R. Han, L. N. Guin, B. Dai, *Consequences of refuge and diffusion in a spatiotemporal predator–prey model*, Nonlinear Anal. Real World Appl., **60** (2021), 36 pages.

[21] E. E. Holmes, M. A. Lewis, J. Banks, R. Veit, *Partial differential equations in ecology: spatial interactions and population dynamics*, Ecology, **75** (1994), 17–29.

[22] S. K. Kar, R. Ransing, S. Y. Arafat, V. Menon, *Second wave of covid-19 pandemic in india: Barriers to effective governmental response*, Clin. Med., **36** (2021), 20 pages.

[23] S. A. Levin, L. A. Segel, *Hypothesis for origin of planktonic patchiness*, Nature, **259** (1976), 659–659.

[24] L. Li, J. Zhen, S. Gui-Quan, *Spatial pattern of an epidemic model with cross-diffusion*, Chinese Phys. Lett., **25** (2008), p. 3500.

[25] Q.-X. Liu, Z. Jin, *Formation of spatial patterns in an epidemic model with constant removal rate of the infectives*, J. Stat. Mech. Theory Exp., **2007** (2007), 13 pages.

[26] B. Liu, R. Wu, L. Chen, *Patterns induced by super cross-diffusion in a predator-prey system with michaelis–menten type harvesting*, Math. Biosci., **298** (2018), 71–79.

[27] H. Liu, Y. Ye, Y. Wei, W. Ma, M. Ma, K. Zhang, *Pattern formation in a reaction-diffusion predator-prey model with weak allee effect and delay*, Complexity, **2019** (2019) 12 pages.

[28] N. Mukherjee, S. Ghorai, M. Banerjee, *Effects of density dependent cross-diffusion on the chaotic patterns in a ratiodependent prey-predator model*, Ecol. Complex., **36** (2018), 276–289.

[29] N. Mukherjee, S. Ghorai, M. Banerjee, *Detection of turing patterns in a three species food chain model via amplitude equation*, Commun. Nonlinear Sci. Numer. Simul., **69** (2019), 219–236.

[30] J. D. Murray, *Mathematical biology II: Spatial models and biomedical applications*, Springer-Verlag, New York, (2001).

[31] S. Riley, K. Eames, V. Isham, D. Mollison, P. Trapman, *Five challenges for spatial epidemic models*, Epidemics, **10** (2015), 68–71.

[32] R. Ruiz-Baier, C. Tian, *Mathematical analysis and numerical simulation of pattern formation under cross-diffusion*, Nonlinear Anal. Real World Appl., **14** (2013), 601–612.

[33] S. Saito, Y. Asai, N. Matsunaga, K. Hayakawa, M. Terada, H. Ohtsu, S. Tsuzuki, N. Ohmagari, *First and second covid-19 waves in japan: a comparison of disease severity and characteristics*, J. Infect., **82** (2021), 84–123.

[34] M. Sambath, K. Balachandran, L. Guin, *Spatiotemporal patterns in a predator-prey model with cross-diffusion effect*, Int. J. Bifurc. Chaos Appl. Sci. Eng., **28** (2018), 13 pages.

[35] G.-Q. Sun, *Pattern formation of an epidemic model with diffusion*, Nonlinear Dynam., **69** (2012), 1097–1104.

[36] G. Sun, Z. Jin, Q.-X. Liu, L. Li, *Pattern formation in a spatial S–I model with non-linear incidence rates*, J. Stat. Mech. Theory Exp., **2007** (2007), 12 pages.

[37] G.-Q. Sun, Z. Jin, Q.-X. Liu, L. Li, *Spatial pattern in an epidemic system with cross-diffusion of the susceptible*, J. Biol. Systems, **17** (2009), 141–152.

[38] A. M. Turing, *The chemical basis of morphogenesis*, Bull. Math. Biol., **52** (1990), 153–197.

[39] T. Wang, *Dynamics of an epidemic model with spatial diffusion*, Phys. A, **409** (2014), 119–129.

[40] W. M. Wang, Y. L. Cai, M. J. Wu, K. Wang, Z. Q. Li, *Complex dynamics of a reaction-diffusion epidemic model*, Nonlinear Anal. Real World Appl., **13** (2012), 2240–2258.

[41] W. Wang, Y. Lin, H. Wang, H. Liu, Y. Tan,*Pattern selection in an epidemic model with self and cross diffusion*, J. Biol. Syst., **19** (2011), 19–31.

[42] W.-M. Wang, H.-W. Liu, Y.-L. Cai, Z.-Q. Li, *Turing pattern selection in a reaction-diffusion epidemic model*, Chin. Phys. B, **20** (2011), p. 074702.

[43] Y. Wang, J. Wang, L. Zhang,*Cross diffusion-induced pattern in an SI model*, Appl. Math. Comput., **217** (2010), 1965–1970.

[44] G. Webb, *A reaction-diffusion model for a deterministic diffusive epidemic*, J. Math. Anal. Appl., **84** (1981), 150–161.

[45] L. Xue, *Pattern formation in a predator-prey model with spatial effect*, Phys. A, **391** (2012), 5987–5996.

[46] S. L. Yuan, C. Q. Xu, T. H. Zhang, *Spatial dynamics in a predator-prey model with herd behavior*, Chaos, **23** (2013), 10 pages.

[47] E. Zemskov, K. Kassner, M. Hauser, W. Horsthemke, *Turing space in reaction-diffusion systems with density-dependent cross diffusion*, Phys. Rev. E, **87** (2013), 12 pages.

[48] E. P. Zemskov, V. K. Vanag, I. R. Epstein, *Amplitude equations for reaction-diffusion systems with cross diffusion*, Phys. Rev E, **84** (2011), 13 pages.

[49] X. C. Zhang, G. Q. Sun, Z. Jin, *Spatial dynamics in a predator-prey model with beddington-deangelis functional response*, Phys. Rev. E, **85** (2012), 11 pages.

[50] T. Zhang, Y. Xing, H. Zang, M. Han, *Spatio-temporal dynamics of a reaction-diffusion system for a predator-prey model with hyperbolic mortality*, Nonlinear Dyn., **78** (2014), 265–277.